

Directing Stem Cell Differentiation via Electrochemical Reversible Switching between Nanotubes and Nanotips of Polypyrrole Array

Yan Wei,^{†,||} Xiaoju Mo,^{†,||} Pengchao Zhang,^{‡,§} Yingying Li,^{‡,§} Jingwen Liao,[⊥] Yongjun Li,^{||} Jinxing Zhang,^{||} Chengyun Ning,[⊥] Shutao Wang,^{*,‡,§} Xuliang Deng,^{*,†} and Lei Jiang^{‡,§}

[†]Department of Geriatric Dentistry, National Engineering Laboratory for Digital and Material Technology of Stomatology, Beijing Laboratory of Biomedical Materials, Peking University School and Hospital of Stomatology, Peking University, Beijing 100081, China

[‡]CAS Key Laboratory of Bio-inspired Materials and Interfacial Science, CAS Center for Excellence in Nanoscience, Technical Institute of Physics and Chemistry, Chinese Academy of Sciences, Beijing 100190, China

[§]School of Future Technology, University of Chinese Academy of Sciences, Beijing 101408, China

[⊥]School of Materials Science and Engineering, South China University of Technology, Guangzhou 510641, China

^{||}Department of Physics, Beijing Normal University, Beijing 100875, China

Supporting Information

ABSTRACT: Control of stem cell behaviors at solid biointerfaces is critical for stem-cell-based regeneration and generally achieved by engineering chemical composition, topography, and stiffness. However, the influence of dynamic stimuli at the nanoscale from solid biointerfaces on stem cell fate remains unclear. Herein, we show that electrochemical switching of a polypyrrole (Ppy) array between nanotubes and nanotips can alter surface adhesion, which can strongly influence mechanotransduction activation and guide differentiation of mesenchymal stem cells (MSCs). The Ppy array, prepared *via* template-free electrochemical polymerization, can be reversibly switched between highly adhesive hydrophobic nanotubes and poorly adhesive hydrophilic nanotips through an electrochemical oxidation/reduction process, resulting in dynamic attachment and detachment to MSCs at the nanoscale. Multicyclic attachment/detachment of the Ppy array to MSCs can activate intracellular mechanotransduction and osteogenic differentiation independent of surface stiffness and chemical induction. This smart surface, permitting transduction of nanoscaled dynamic physical inputs into biological outputs, provides an alternative to classical cell culture substrates for regulating stem cell fate commitment. This study represents a general strategy to explore nanoscaled interactions between stem cells and stimuli-responsive surfaces.

KEYWORDS: polypyrrole, electrochemical switching, nanotube/nanotip array, stem cell differentiation, smart surface



Stem-cell-based regeneration holds great promise for treating aged, injured, and diseased tissues, but control of cell fate remains a great challenge.^{1–5} Material-based biointerfaces with moderate biomimetic environmental cues offer a prospective means to define cell differentiation, in addition to complex soluble chemistry and genetic reprogramming. Seminal biointerfaces in this field with properties static in time, generally achieved by engineering chemical composition,^{6,7} topography,^{8–11} and stiffness,^{12–14} have demonstrated their capability to regulate stem cell behaviors. Although previous studies have highlighted the importance of cell-surface interactions in determining cell fate, those engineered biointerfaces often inadequately mimic the dynamic features of the extracellular matrix.

Recently, several elaborate dynamic solid biointerfaces have enabled successful influence on cell behaviors,^{15–19} such as

sensing,^{20,21} adhesion,^{22,23} and migration.^{24,25} For example, stimuli-presentable peptide surfaces^{26,27} majored in chemical adjustment at molecular level. Some other attempts have focused on stiffness regulation from macro/microscale, such as stretchable parafilms with microgrooves,²⁸ photodegradable hydrogels,²⁹ and magnetic-tunable plastic surfaces.³⁰ However, the performance and design of those artificial biointerfaces lagged behind natural niches that can provide reversibly physical and chemical stimuli. Furthermore, natural stem cells *in vivo* exist in a dynamic environment in which they are exposed to nanoscale stimuli. They can use their nano-components (such as self-assembly of integrin, actin, or

Received: March 8, 2017

Accepted: June 6, 2017

Published: June 6, 2017

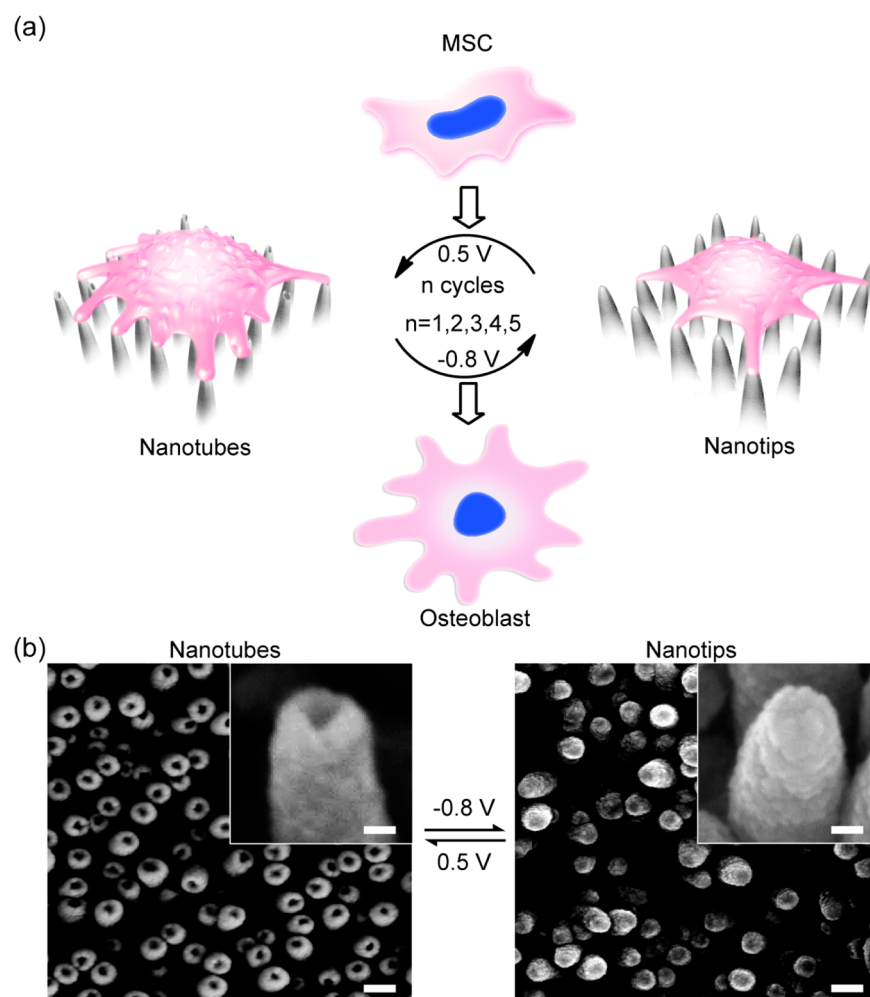


Figure 1. Electrochemical switchable nanotube/nanotip transition of Ppy arrays guides stem cell fate commitment. (a) Schematic illustration of the nanotube/nanotip transition on a Ppy array directing MSC behavior in response to multiple cycles of electrochemical redox switching. (b) Field-emission scanning electron microscopy images of Ppy arrays at different redox states. Electrochemical redox switching results in contraction (oxidized) and expansion (reduced) of Ppy, which produces variation of the inner diameter. Scale bars, 100 nm. The insets show magnified nanotubes and nanotips. Scale bars, 20 nm.

proteins) to sense and transduce surface signals to manipulate cellular behavior. Therefore, it is a great challenge to establish a niche-like artificial nanobiointerface to regulate stem cell fate.

Here, we developed a smart nano-biointerface with an electrochemically switchable polypyrrole (Ppy) array to provide dynamic nanoscale stimuli to guide stem cell osteogenic fate commitment (Figure 1a). The Ppy array was engineered using a template-free electrochemical polymerization technique.³¹ Reversibly switching the Ppy array between nanotubes and nanotips *via* electrochemical reduction/oxidation transforms it from a highly adhesive hydrophobic surface to poorly adhesive hydrophilic surface and *vice versa*. Thus, nanotube/nanotip switching provides dynamic attachment and detachment stimuli to favor and disrupt mesenchymal stem cell (MSC) adhesion at the nanoscale. Furthermore, multicyclic attachment/detachment achieved using Ppy array can initiate intracellular mechanotransduction, mediated by YAP/RUNX2, cytoskeleton organization, and MSC osteogenesis independent of surface stiffness and additional chemical inducers.

RESULTS AND DISCUSSION

Ppy Nanotube Array Fabrication and Electrochemically Reversible Redox Switching. We engineered a

conducting Ppy nanotube array on titanium substrates using a template-free electrochemical polymerization approach. As a classical conducting polymer, Ppy is often selected for smart biointerfaces^{32–34} because of its excellent electrochemical properties^{35,36} and biocompatibility.^{37,38} The redox reversibility of the as-produced Ppy array was evidenced by the good x axis symmetry of its cyclic voltammetry curves (Figure S1), which had an oxidation peak at 0.12 V and a reduction peak at -0.38 V. Therefore, we selected 0.5 V/ -0.8 V as the oxidation/reduction switch potentials to offer an accurate temporal control. Direct observation using field-emission scanning electron microscopy (FE-SEM) revealed that the Ppy array had nanotube morphology in the oxidized state and had a nanotip appearance in the reduced state (Figure 1b and Figure S2a,c). The nanotubes and nanotips of the Ppy array have similar random arrangement. However, the hollow inner spaces (24 ± 4 nm at the top area) at the tops of nanotubes were almost invisible on nanotips. This inner diameter of nanotubes has been reported to accelerate focal contact formation and enhance cellular activities.³⁹ Characterization of the morphology of Ppy array by *in situ* atomic force microscopy (AFM) verified the reversibility of the morphological transition between nanotubes and nanotips, as indicated by a series of *in situ*

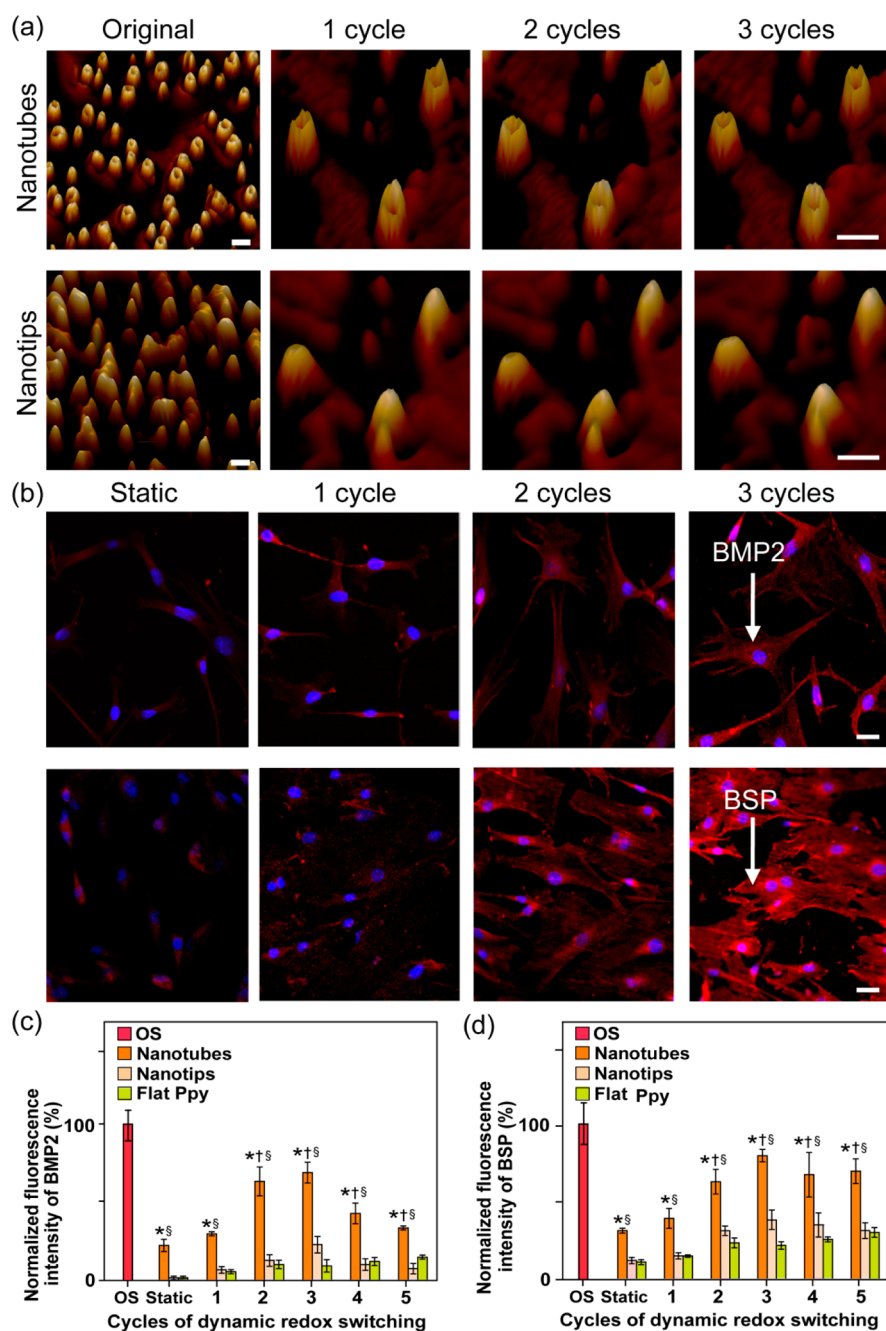


Figure 2. Reversibility of the nanotube/nanotip transition and its cycle-dependent effects on directing osteogenic differentiation of MSCs. (a) Atomic force microscopy phase images in tapping mode, showing the reversible nanotube/nanotip transition due to electrochemical redox switching. Scale bars for original images, 100 nm. Scale bars for the images taken after 1–3 cycles, 20 nm. (b) Immunostaining for osteogenic proteins BMP2 (top) and BSP (bottom) in MSCs cultured on nanotubes for 7 days after experiencing various numbers of cycles of the nanotube/nanotip transition. Static and 1 cycle note the weak staining of BMP2/BSP; 2 cycles and 3 cycles note the osteoblastic morphology and bright staining of BMP2/BSP. Scale bars, 20 μm . Quantification of the mean immunofluorescence intensity of (c) BMP2 and (d) BSP; the intensity was normalized to that of the positive control group, which consisted of MSCs that were chemically induced with an osteogenic supplement (OS). The highest intensity for BMP2 and BSP was recorded in MSCs cultured on nanotubes. The intensity of BMP2 and BSP increased approximately linearly after 1, 2, and 3 cycles, but it decreased markedly after 4 and 5 cycles; * $p < 0.01$ vs corresponding flat Ppy group; $^{\S}p < 0.01$ vs the corresponding nanotips group; $^{\ddagger}p < 0.05$ vs the static nanotubes group. BMP2, red; BSP, red.

AFM phase images collected in tapping mode (Figure 2a and Figure S3). The transition between nanotubes and nanotips should be ascribed to the volume expansion/contraction of Ppy, related to insertion/expulsion of ions.^{40–42} Upon exposure to a reducing potential, anions (e.g., PO_4^{3-} , H_2PO_4^-) in the surrounding PBS electrolytes enter the Ppy and cause it to expand to occupy the spaces within the nanotubes, resulting in

nanotips. Upon exposure to an oxidizing potential, ions exit Ppy, and it contracts to unoccupy the inner space of nanotips, yielding nanotubes. Therefore, we have achieved a smart Ppy array surface that can provide reversible stimuli *via* electrochemical redox switching between nanotubes and nanotips.

Impact of Ppy Nanotube/Nanotip Switching on MSC Differentiation. To investigate the influence of nanoscale

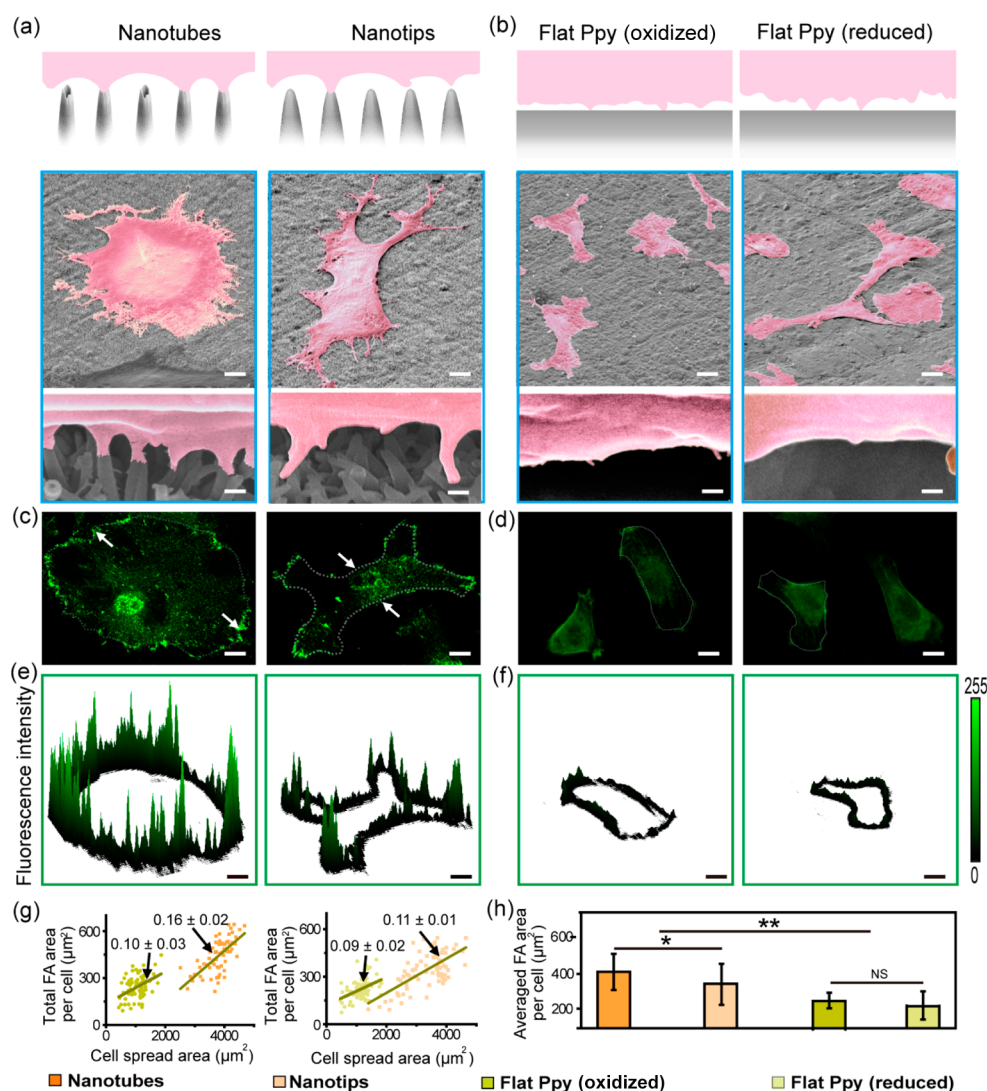


Figure 3. Nanotube/nanotip transition can favor and disrupt MSCs' adhesion at the nanoscale. (a,b) Schematic illustration and representative SEM images of FA. (c,d) Representative immunofluorescence profiles of FAs. (e,f) Three-dimensional fluorescence intensity profiles of boundary FAs (location indicated by dashed white lines in the corresponding images in (c) and (d)). The fluorescence intensity is indicated in arbitrary fluorescent units. (g) Correlative analysis of total FA area/cell spread area. (h) Quantitative analysis of the averaged FA area per cell. Each data point represents an individual cell (279 cells were analyzed). Data trends in (g) are plotted and compared with the linear least-squares fitting (dark yellow lines, slope values are indicated). NS, not significant; * $p < 0.05$; ** $p < 0.01$. Bars: (a,b) scale bars in top row, 10 μm ; scale bars in bottom row, 100 nm. (c–f) scale bars, 10 μm .

reversible stimuli on cell fate, we observed MSC differentiation on the Ppy array during the nanotube/nanotip transition. We monitored changes in the expression of two typical osteogenic biomarkers, bone morphogenetic protein 2 (BMP2) and bone sialoprotein (BSP),^{43,44} in MSCs after varied cycles of reversible nanotube/nanotip transition and seven subsequent days of cell culture (Supporting Information section 5 and Figure S4).²⁷ The fluorescence intensities of BMP2 and BSP on Ppy nanotubes were closely related to the number of cycles of the nanotube/nanotip transition (Figure 2). From one to three cycles, the increased fluorescence intensities of BMP2 and BSP indicated that MSC differentiation was gradually biased toward osteogenesis. However, increasing the number of cycles to five decreased the fluorescence intensities of BMP2 and BSP (Figure S5a,b) and reduced cell density (Figure S6), which might be ascribed to dissociation of the cell material connection caused by excessive stimulation.⁴⁵ Then, the significantly upregulated gene expression of BMP2 and BSP (Figure S7)

and the obvious osteoid formation (Figure S8) further demonstrated that three cycles of dynamic nanotube/nanotip transition obviously promoted osteogenic differentiation, although this method was slightly less effective than chemical induction with osteogenic supplement (OS) (Figure S5c). On Ppy nanotips, the fluorescence intensities of BMP2 and BSP were significantly lower than those on the nanotubes of the corresponding group, and there was a continuous decrease in cell densities as the number of cycles of dynamic nanotube/nanotip transition increased. On flat Ppy surfaces, the very weak fluorescence intensities of BMP2 and BSP were observed after corresponding cycles of electrochemical redox switching, suggesting the importance of nanostructures in influencing stem cell fate. On the static Ppy nanotube array, weak fluorescence intensities of BMP2 and BSP were also observed, indicating the limited influence of static nanostructures. These results indicate that the electrochemical switched nanotube/nanotip transition of the Ppy nanotube array can direct MSCs

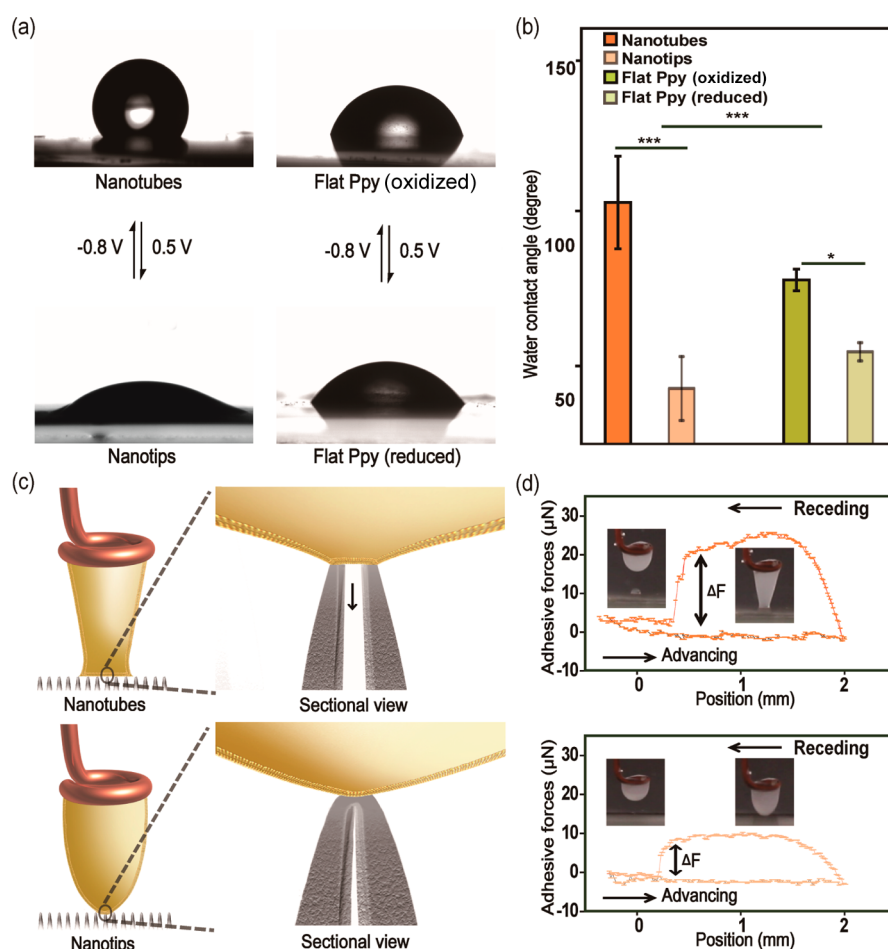


Figure 4. Transition between highly adhesive hydrophobic nanotubes and poorly adhesive hydrophilic nanotips acts as dynamic attachment/detachment stimulus. (a) Nanotube/nanotip transition causes significant changes in hydrophilicity of the Ppy array. (b) Quantification of water contact angles. (c) Schematic illustration of the different phospholipid adhesive mode of nanotubes and nanotips. When a phospholipid droplet on the top area of nanotubes pulls upward, capillary adhesion forces arise to maintain the pressure balance of the inner space. In contrast, no capillary force is present on nanotips because the inner space is closed. (d) Quantification of phospholipid adhesive forces. ΔF is the stretching force measured between the Ppy substrates and the phospholipid droplet. The adhesive force on nanotubes ($20.8 \pm 2.1 \mu\text{N}$) was significantly higher than that on the nanotips ($9.7 \pm 1.6 \mu\text{N}$). NS, not significant; * $p < 0.05$; *** $p < 0.001$.

toward osteogenic differentiation with effectiveness comparable to that of chemical agents. In addition, the number of cycles of nanotube/nanotip switching plays a critical role in guiding MSC osteogenesis.

Cell-Surface Interactions on Ppy Nanotube/Nanotip Arrays. To clarify the initial cellular responses to the nanotube/nanotip transition on the Ppy array, we observed cell-surface interactions using SEM and confocal laser scanning microscopy (CLSM). Focal adhesions (FAs) at the cell-substrate interface provide a location for transmission of signals for cell survival, proliferation, and differentiation.⁴⁶ Representative SEM images show that cell filopodia can attach onto the tops and sides of nanotubes but are only partially attached to the nanotips (Figure 3a and Figure S9a,c). In contrast, few apparent filopodia extend from cells onto flat Ppy surfaces in either redox states (Figure 3b and Figure S9b,d). Thus, the electrochemically switched transition between nanotubes and nanotips on the Ppy array could provide pointwise nanoscale contact guidance to finely control MSC adhesion. Representative immunofluorescence profiles of FAs (Figure 3c and Figure S10a) and three-dimensional fluorescence intensity profiles of boundary FAs (Figure 3e) show that the abundance of FAs on Ppy nanotubes decreased markedly when the nanotubes were

transformed into nanotips. In contrast, few FAs were observed on flat Ppy surfaces, and these FAs showed no apparent response to electrochemical redox switching (Figure 3d,f and Figure S10b). Furthermore, correlative analysis of the total FA area/cell spread area (Figure 3g) and quantitative analysis of the averaged FA area per cell (Figure 3h) showed that the FAs on nanotubes were larger than those on the nanotips. In comparison, on flat Ppy surfaces, the total FA areas in the oxidized state are similar to those in the reduced state. The total FA areas on the Ppy array were larger than those on flat Ppy surfaces, suggesting that the nanotube array provided more anchoring points for FAs to facilitate cell adhesion. These statistical analyses, which were based on a large number of cells, showed trends similar to those found in the observation of individual cells *via* SEM and CLSM. Collectively, our findings suggest that electrochemical switching of the nanotube/nanotip transition on the Ppy array can favor and disrupt MSCs' adhesion at the nanoscale.

Variation in Surface Properties with Nanotube/Nanotip Switching. To identify the physical chemistry mechanisms underlying the different cell-surface interactions triggered by the dynamic Ppy array, we assessed variation in the surface properties of such an array, including wettability, adhesive force,

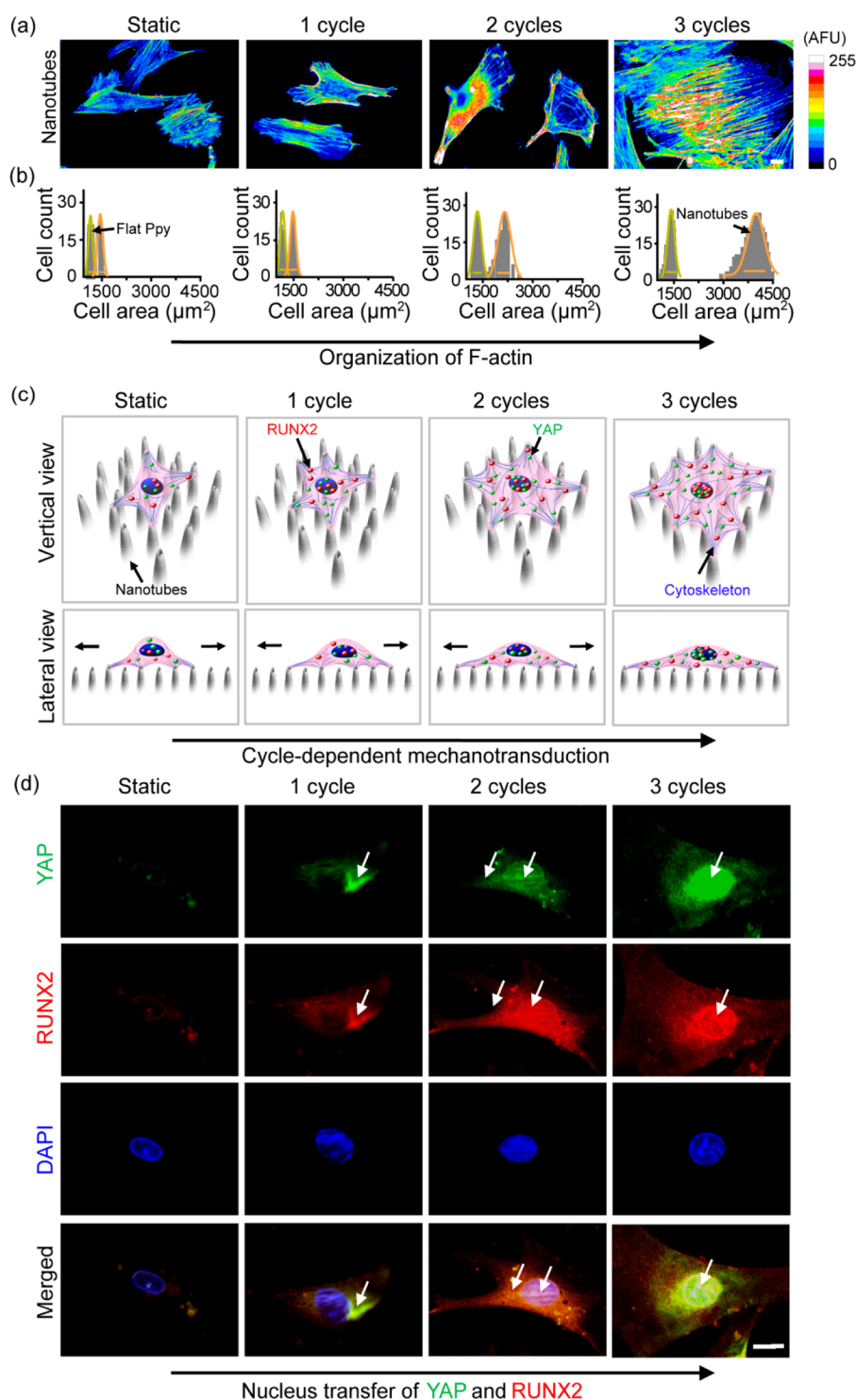


Figure 5. Dynamic attachment/detachment stimuli activate both structural and molecular signaling underlying MSC mechanotransduction. (a) Background-subtracted fluorescence images (pseudocolored heat maps) of actin filaments. Scale bars, 10 μm . (b) Distribution of MSC area after experiencing various numbers of cycles of attachment/detachment. Gaussian functions (orange curves for nanotubes and green curves for flat Ppy) were used for fitting. Bars (orange for nanotubes and green for flat Ppy) are centered on the mean and indicate peak widths. (c) Schematic illustration of nuclear translocation of YAP/RUNX2 and F-actin organization promoted by cyclic attachment/detachment. (d) Fluorescent images of YAP/RUNX2 nucleus revealing significantly enhanced nuclear translocation (activation) as the number of cycles of attachment/detachment increased. YAP, green; RUNX2, red; DAPI, blue. Scale bars, 10 μm .

electric potential, and elastic modulus, during nanotube/nanotip switching. The changes in water contact angles (Figure 4a,b) of the Ppy array ($105 \pm 15^\circ$ for nanotubes vs $44 \pm 10^\circ$ for nanotips) during redox switching were much larger than those of flat Ppy surfaces ($79 \pm 3^\circ$ for oxidation vs $56 \pm 3^\circ$ for

reduction). It has been well-established that hydrophobicity facilitates cell adhesion,⁴⁷ whereas hydrophilicity inhibits cell-surface interaction.^{48,49} Thus, the capacity for dynamic transformation between hydrophobic nanotubes and hydrophilic nanotips may provide the Ppy array with the capability to

dynamically regulate cell-surface interactions. To test this possibility, we investigated the underwater adhesive force on the Ppy surfaces, using a phospholipid (the main component of cellular membrane) droplet as a simplified cell model. It should be noted that a significantly higher underwater adhesive force was obtained on nanotubes ($20.8 \pm 2.1 \mu\text{N}$) in comparison with that measured on nanotips ($9.7 \pm 1.6 \mu\text{N}$). Additionally, similar variation of adhesive forces was achieved in cell culture medium (Figure S12). These phenomena might be ascribed to the capillary adhesive force of nanotubes (Figure 4c,d).⁵⁰ In comparison, no significant difference was observed between the adhesive forces of flat Ppy surfaces in oxidized state ($5.3 \pm 0.6 \mu\text{N}$) and reduced state ($5.1 \pm 0.8 \mu\text{N}$) (Figure S11a), indicating that no capillary force was present on the surface lacking nanotubes. These results demonstrate that nanotube/nanotip switching could lead to variation in underwater affinity of Ppy arrays for cell membrane components, which would allow dynamic regulation of cell-surface interactions. For the elastic modulus, no significant variations were observed (Figure S11b) between values measured during oxidation and reduction switching for Ppy arrays ($156 \pm 22 \text{ MPa}$ vs $160 \pm 26 \text{ MPa}$) or flat Ppy surfaces ($556 \pm 38 \text{ MPa}$ vs $579 \pm 57 \text{ MPa}$), and a high elastic modulus has been reported to favor cell spreading and osteogenesis.^{51,52} For surface electrical potential, little variations were observed in response to oxidation/reduction switching (Figure S11c) for the Ppy arrays ($-0.31 \pm 0.03 \text{ mV}$ vs $-0.53 \pm 0.05 \text{ mV}$) and flat Ppy surfaces ($-0.34 \pm 0.03 \text{ mV}$ vs $-0.59 \pm 0.05 \text{ mV}$). Thus, the reversible transition between highly adhesive hydrophobicity and poorly adhesive hydrophilicity, corresponding to nanotube/nanotip switching, allows the application of dynamic stimuli to manipulate MSCs' surface adhesion from the nanoscale.

Transduction of Nanotube/Nanotip Switching into Intracellular Biological Signals. To explore how the stimulus of cyclic attachment/detachment of the Ppy array was further transduced by MSCs, we directly observed downstream intracellular structural rearrangements. For MSCs on the Ppy array, actin filament organization (Figure 5a and Figure S13) and cell spread areas (Figure 5b) were gradually increased as the number of cycles (from 1 to 3) of dynamic attachment/detachment was increased from 1 to 3, but these properties changed little in MSCs on corresponding flat Ppy surfaces. These results reveal that cyclic attachment/detachment on cell surfaces can promote cytoskeleton rearrangements and confirm the sensitivity of the cytoskeleton to nanoscale dynamic stimuli in addition to macroscale mechanical stretching and fluid flow shearing.^{53,54} With anchor points at FAs, the cytoskeleton is a sensitive detector of extracellular nanoscale dynamic stimuli. Furthermore, because the cytoskeleton is physically coupled with FAs and nucleus,^{55,56} cytoskeleton filaments directly facilitate the conversion of external attachment/detachment stimuli into nuclear signals. These results suggest that the electrochemical switching of the nanotube/nanotip transition on the Ppy array could activate cytoskeleton-mediated mechanotransduction (Figure 5c).

We further investigated the mechanotransduction related proteins, Yes associated protein (YAP), and preosteogenic Runt related transcription factor 2 (RUNX2), in MSCs during electrochemical switching of the nanotube/nanotip transition on Ppy arrays. YAP, a critical outside-in mechanotransduction mediator, can translate physical information into protein expression by localizing to the nucleus.^{57,58} RUNX2, a transcriptional partner of YAP, can be coactivated along with

YAP to initiate osteogenesis.^{59,60} Fluorescent images (Figure 5d and Figure S14a) and quantitative analysis (Figure S14b) of changes in YAP/RUNX2 expression patterns revealed that nuclear translocation of YAP/RUNX2 was significantly increased for three nanotube/nanotip transition cycles. Without dynamic attachment/detachment stimuli, little YAP and RUNX2 staining was observed in the cytoplasm, indicating that these proteins were generally in a deactivated state. Upon one cycle of dynamic attachment/detachment, enhanced nuclear localization (activation) of YAP and RUNX2 was observed in MSCs, which indicated that outside-in physicochemical signal transduction was initiated. Three cycles of attachment/detachment achieved the highest gene expression (Figure S7) and the highest nuclear translocation of YAP ($65 \pm 5\%$ nucleus localized) and RUNX2 ($39 \pm 6\%$ nucleus localized), which demonstrated significant activation of mechanotransduction. Furthermore, increasing the number of cycles of attachment/detachment led to partial deactivation of YAP and RUNX2, suggesting that the mechanotransduction was weakened because of decreased binding of MSCs caused by excessive stimulation. These cycle-dependent activation trends of YAP/RUNX2 upon the dynamic attachment/detachment stimuli are in accordance with those of osteogenic proteins BMP2 and BSP. To confirm the functional role of YAP/RUNX2 in the process of MSC differentiation regulated by changes on nanotube array surfaces, we reduced YAP expression using short hairpin RNAs (shRNAs). We found that knocking down YAP signaling significantly suppressed RUNX2 expression in MSCs on nanotubes (Figure S15). These results suggest that dynamic attachment/detachment stimuli of the Ppy array could activate the nuclear translocation of mechanotransducer YAP to promote intranuclear RUNX2 transcription (Figure 5c).

CONCLUSION

In conclusion, we demonstrate that electrochemical reversible switching of the Ppy array between nanotubes and nanotips can strongly influence MSCs' fate commitment. The transition between highly adhesive hydrophobic nanotubes and poorly adhesive hydrophilic nanotips provides cyclic attachment/detachment to cells. This dynamic nanoscale switching could be used to direct osteogenic differentiation of MSCs in a cycle-dependent manner. Further, we showed that intracellular mechanotransduction mediated by YAP/RUNX2 and cytoskeleton organization in MSCs might be mechanisms through which nanoscaled dynamic stimuli induce osteogenesis. This strategy for designing smart biointerfaces can be extended to other stimuli-responsive materials friendly to stem cells for future tissue regeneration.

MATERIALS AND METHODS

Materials. Electrical-responsive nanotube array surfaces and flat Ppy surfaces were prepared by template-free electrochemical polymerization using an electrochemical station (Zennium Zahner, Germany). Cyclic voltammetry (CV) was measured using an electrochemical station (Zennium Zahner, Germany). Two-dimensional surface morphology characterization was performed using a field-emission scanning electron microscope (ZEISS Ultra 55, Germany). Three-dimensional morphology characterization and quantitative nanomechanical property mapping (QNM) measurements were carried out using AFM (Bruker, Dimension Icon, USA). Surface potentials were measured via AFM (Bruker, Multimode 8, USA) in a surface potential mode. Surface contact angle (SCA) analysis was performed using a SCA analyzer (Filderstadt OCA15, Germany) at ambient

temperature. Bone marrow mesenchymal stem cells (RASM-01001, USA) and MSC basal medium were supplied by Cyagen Bioscience Inc. Fluorescence microscopy images were achieved using a laser scanning confocal microscope (Zeiss, LSM 780, Germany) and analyzed using ImageJ software (National Institutes of Health, Bethesda, MD, USA) (<http://rsb.info.nih.gov/ij>) and Image Pro Plus 3.1 software (Media Cybernetics). Droplet digital PCR reading was performed using a Bio-Rad QX200 droplet digital PCR system (Bio-Rad, USA).

Preparation of Ppy Surfaces. The small electrochemical cell included a biomedical titanium sheet (effective area of 10 mm × 10 mm) as a working electrode, a copper sheet as a counter electrode, saturated calomel electrode (SCE) as a reference electrode, and an electrolyte (0.2 M KCl solution containing 0.1 M pyrrole monomer). The titanium sheet (*i.e.*, the working electrode) was immersed into the electrolyte. Then the Ppy prenucleation film was formed on the working electrode at 0.8 V (*vs* SCE) for 20 s at room temperature under the control of an electrochemical station. The as-produced Ppy prenucleation substrates were immersed in an electrolyte-rich phosphate buffer solution (PBS, 0.5 M, physiological pH value) containing 0.2 M Py and 0.01 M naphthalene sulfonic acid. The Ppy nanotube array (pH 6.8) and flat Ppy surfaces (pH 5.7) were galvanostatically (0.9 mA/cm² for 7 min) fabricated on the Ppy prenucleation substrates. The as-obtained products were rinsed several times in deionized water and dried under vacuum.

Characterization Methods and Settings. *Electrochemical Redox Switching of Ppy Surfaces.* To evaluate the redox potentials of the as-produced nanotube array and flat Ppy surfaces, CV was performed using an electrochemical station with electrolytes (mesenchymal stem cell basal medium, pH 6.8), a biomedical titanium sheet (deposited with nanotube array surfaces and flat Ppy surfaces) as a working electrode, a platinum electrode as a counter electrode, and a SCE as a reference electrode. The CV curves were recorded by applying a scanning potential from +0.8 V to −1.0 V at a scan rate of 20 mV/s. According to the CV curves, we determined that the reduction and oxidation potentials of the Ppy array were −0.38 V and +0.12 V, respectively, whereas those of the flat Ppy surface were −0.38 V and +0.24 V, respectively.

Morphology Characterization. We used specially adapted tissue culture plates (TCPs) to apply −0.80 V (reduction potential) or +0.5 V (oxidation potential) to trigger redox reactions on nanotube array surfaces and flat Ppy surfaces (working electrode) for 20 min. FE-SEM (5 kV acceleration voltage) was employed to examine the two-dimensional surface morphology of the nanotube array and flat Ppy surfaces at different redox states. The three-dimensional morphology of the nanotube array and flat Ppy surfaces was characterized at different redox states using AFM in tapping mode. In order to obtain high-resolution images, an OTESPA probe with a spring constant of approximately 40 N/m was used to capture the images. Phase images were taken at scanning rates of approximately 1.5 Hz.

Surface Wettability Characterization. The surface wettability of the nanotube array and flat Ppy surfaces that experienced redox switching was evaluated by SCA analysis of 2 μL water droplets on the samples using a surface contact angle analyzer at ambient temperature.

Surface Potential Characterization. Surface potential of the nanotube array and flat Ppy surfaces was measured *via* AFM (in surface potential mode) with Pt-coated Si tips with a spring constant of approximately 5 N/m (SCM-PIT, Bruker, USA). The typical tip velocity was 2 μm/s.

Nanomechanical Property Characterization. The mechanical properties of the nanotube array and flat Ppy surfaces were determined by QNM as described in our previous work.¹ A ScanAsyst-Air tip (Bruker, USA) with a spring constant of approximately 0.4 N/m and an OTESPA tip (Bruker, USA) with a spring constant of 40 N/m were used for QNM imaging of the nanotube array and flat Ppy surfaces, respectively. The effective modulus was calculated by extrapolating the retraction curve close to the contact point and using a Derjaguin–Muller–Toporov (DMT) model (eq 1):

$$F_{\text{tip}} - F_{\text{adh}} = \frac{4}{3} E^* \sqrt{Rd^3} \quad (1)$$

where F_{tip} is the loading force, F_{adh} is the adhesion force, E^* is the reduced Young's modulus, R is the tip radius, and d is the deformation depth. E can be calculated from E^* and Poisson's ratio of the sample and the tip.

MSC Culture. MSCs were thoroughly characterized as previously described.^{2,27,61} MSCs adherent on tissue culture plates were maintained in MSC basal medium (containing 10% MSC-qualified fetal bovine serum, 10 μg/mL glutamine, and 100 IU/mL penicillin-streptomycin). The medium was changed every 2–3 days. At 80–90% confluence, MSCs were detached with 0.25% trypsin/EDTA (Gibco). Early passages of MSCs were used in this study (passages 3–6).

Applying Dynamic Stimuli to MSCs by Switching of Ppy Nanotubes/Nanotips. Briefly, MSCs (1 × 10⁴ cells/well) were seeded onto a nanotube array and flat Ppy surfaces in 24-well plates specifically modified for applying potentials as in Figure S4. The seeded MSCs were incubated at 37 °C in a humidified atmosphere containing 5% CO₂. MSC basal medium without osteogenic supplement was used for cell culture to remove any confounding effect of chemical agents and to explore how local stimuli prime cells in a noninducing landscape. After 1 day of culture to allow cell–substrate attachment, varying numbers of cycles of redox electrical potentials were applied to substrates. Experimental conditions are labeled according to the number of cycles of applied redox switching potential, such that 1 cycle corresponds to one instance of reduction/oxidation (close with −0.80 V/20 min, open with 0.5 V/20 min). After each cycle of redox switching, the samples were immediately fixed for characterization of FAs, mechanical mediator YAP, preosteogenic transcription factor RUNX2, and F-actin. After 7 days of culture following the regular model of stem cell differentiation,⁶² the samples were fixed for immunocytochemistry assay to detect osteogenic proteins BMP2 and BSP. MSCs cultured on TCPs with osteogenic inducing medium were used as positive control cells.

Cell Attachment and Proliferation Assay. The cell attachment morphology of MSCs was observed using SEM at 15 kV. The as-obtained samples were fixed in 2.5% glutaraldehyde, dehydrated in a series of increasing concentrations of ethanol, air-dried in a force-air hood, sputtered with gold, and imaged *via* SEM.

ShRNA Knockdown of YAP. To generate YAP knockdown cells, MSCs were transfected with lentivirus containing shRNA targeting YAP. In a parallel control experiment, MSCs were transfected with nontargeted control shRNA. After transfection, MSCs were plated on Ppy substrates. Samples were harvested for immunocytochemistry analysis after they were subjected to varying numbers of cycles of redox switching.

ASSOCIATED CONTENT

Supporting Information

The Supporting Information is available free of charge on the ACS Publications website at DOI: 10.1021/acsnano.7b01661.

Experimental details and supplementary figures (PDF)

AUTHOR INFORMATION

Corresponding Authors

*E-mail: stwang@mail.ipc.ac.cn.

*E-mail: kqdengxuliang@bjmu.edu.cn.

ORCID

Shutao Wang: 0000-0002-2559-5181

Lei Jiang: 0000-0003-4579-728X

Author Contributions

[¶]Y.W. and X.M. contributed equally to this work.

Notes

The authors declare no competing financial interest.

ACKNOWLEDGMENTS

This research acknowledges support from the FokYing Tung Education Foundation (151034), the Beijing Nova Program (No. Z14111000180000), National Natural Science Foundation of China (21425314, 81425007, 31570990, and 31670993), the Top-Notch Young Talents Program of China, and the Key Research Program of the Chinese Academy of Sciences (KJZD-EW-M01).

REFERENCES

- (1) Li, Y. J.; Wang, J. J.; Ye, J. C.; Ke, X. X.; Gou, G. Y.; Wei, Y.; Xue, F.; Wang, J.; Wang, C. S.; Peng, R. C.; et al. Mechanical Switching of Nanoscale Multiferroic Phase Boundaries. *Adv. Funct. Mater.* **2015**, *25*, 3405–3413.
- (2) Zhang, X. H.; Xu, M. M.; Song, L.; Wei, Y.; Lin, Y. H.; Liu, W. T.; Heng, B. C.; Peng, H.; Wang, Y.; Deng, X. L. Effects of Compatibility of Deproteinized Antler Cancellous Bone with Various Bioactive Factors on Their Osteogenic Potential. *Biomaterials* **2013**, *34*, 9103–9114.
- (3) Liu, X.; Wang, S. Three-dimensional Nano-Biointerface As a New Platform for Guiding Cell Fate. *Chem. Soc. Rev.* **2014**, *43*, 2385–2401.
- (4) Cosgrove, B. D.; Mui, K. L.; Driscoll, T. P.; Caliarì, S. R.; Mehta, K. D.; Assoian, R. K.; Burdick, J. A.; Mauck, R. L. N-Cadherin Adhesive Interactions Modulate Matrix Mechanosensing and Fate Commitment of Mesenchymal Stem Cells. *Nat. Mater.* **2016**, *15*, 1297–1306.
- (5) Green, J. J.; Elisseff, J. H. Mimicking Biological Functionality with Polymers for Biomedical Applications. *Nature* **2016**, *540*, 386–394.
- (6) Villa-Diaz, L. G.; Nandivada, H.; Ding, J.; Nogueira-de-Souza, N. C.; Krebsbach, P. H.; O'Shea, K. S.; Lahann, J.; Smith, G. D. Synthetic Polymer Coatings for Long-Term Growth of Human Embryonic Stem Cells. *Nat. Biotechnol.* **2010**, *28*, 581–583.
- (7) Kilian, K. A.; Mrksich, M. Directing Stem Cell Fate by Controlling the Affinity and Density of Ligand-Receptor Interactions at the Biomaterials Interface. *Angew. Chem., Int. Ed.* **2012**, *51*, 4891–4895.
- (8) Chen, C. S.; Mrksich, M.; Huang, S.; Whitesides, G. M.; Ingber, D. E. Geometric Control of Cell Life and Death. *Science* **1997**, *276*, 1425–1428.
- (9) McMurray, R. J.; Gadegaard, N.; Tsimbouri, P. M.; Burgess, K. V.; McNamara, L. E.; Tare, R.; Murawski, K.; Kingham, E.; Oreffo, R. O.; Dalby, M. J. Nanoscale Surfaces for the Long-Term Maintenance of Mesenchymal Stem Cell Phenotype and Multipotency. *Nat. Mater.* **2011**, *10*, 637–644.
- (10) Yao, X.; Peng, R.; Ding, J. Cell-Material Interactions Revealed via Material Techniques of Surface Patterning. *Adv. Mater.* **2013**, *25*, 5257–5286.
- (11) Dalby, M. J.; Gadegaard, N.; Oreffo, R. O. Harnessing Nanotopography and Integrin-Matrix Interactions to Influence Stem Cell Fate. *Nat. Mater.* **2014**, *13*, 558–569.
- (12) Yang, C.; Tibbitt, M. W.; Basta, L.; Anseth, K. S. Mechanical Memory and Dosing Influence Stem Cell Fate. *Nat. Mater.* **2014**, *13*, 645–652.
- (13) Wen, J. H.; Vincent, L. G.; Fuhrmann, A.; Choi, Y. S.; Hribar, K. C.; Taylor-Weiner, H.; Chen, S.; Engler, A. J. Interplay of Matrix Stiffness and Protein Tethering in Stem Cell Differentiation. *Nat. Mater.* **2014**, *13*, 979–987.
- (14) Das, R. K.; Gocheva, V.; Hammink, R.; Zouani, O. F.; Rowan, A. E. Stress-Stiffening-Mediated Stem-Cell Commitment Switch in Soft Responsive Hydrogels. *Nat. Mater.* **2015**, *15*, 318–325.
- (15) Mager, M. D.; LaPointe, V.; Stevens, M. M. Exploring and Exploiting Chemistry at the Cell Surface. *Nat. Chem.* **2011**, *3*, 582–589.
- (16) Sun, T.; Qing, G. Biomimetic Smart Interface Materials for Biological Applications. *Adv. Mater.* **2011**, *23*, H57–H77.
- (17) Wu, Y. L.; Putcha, N.; Ng, K. W.; Leong, D. T.; Lim, C. T.; Loo, S. C. J.; Chen, X. D. Biophysical Responses upon the Interaction of

Nanomaterials with Cellular Interfaces. *Acc. Chem. Res.* **2013**, *46*, 782–791.

(18) Shah, S.; Solanki, A.; Lee, K. B. Nanotechnology-Based Approaches for Guiding Neural Regeneration. *Acc. Chem. Res.* **2016**, *49*, 17–26.

(19) Chaudhuri, O.; Gu, L.; Klumpers, D.; Darnell, M.; Bencherif, S. A.; Weaver, J. C.; Huebsch, N.; Lee, H. P.; Lippens, E.; Duda, G. N.; Mooney, D. J. Hydrogels with Tunable Stress Relaxation Regulate Stem Cell Fate and Activity. *Nat. Mater.* **2015**, *15*, 326–334.

(20) Baker, B. M.; Trappmann, B.; Wang, W. Y.; Sakar, M. S.; Kim, I. L.; Shenoy, V. B.; Burdick, J. A.; Chen, C. S. Cell-Mediated Fibre Recruitment Drives Extracellular Matrix Mechanosensing in Engineered Fibrillar Microenvironments. *Nat. Mater.* **2015**, *14*, 1262–1268.

(21) Hanson, L.; Zhao, W. T.; Lou, H. Y.; Lin, Z. C.; Lee, S. W.; Chowdary, P.; Cui, Y.; Cui, B. X. Vertical Nanopillars for *in situ* Probing of Nuclear Mechanics in Adherent Cells. *Nat. Nanotechnol.* **2015**, *10*, 554–562.

(22) Fu, J. P.; Wang, Y. K.; Yang, M. T.; Desai, R. A.; Yu, X. A.; Liu, Z. J.; Chen, C. S. Mechanical Regulation of Cell Function with Geometrically Modulated Elastomeric Substrates. *Nat. Methods* **2010**, *7*, 733–736.

(23) Gjorevski, N.; Sachs, N.; Manfrin, A.; Giger, S.; Bragina, M. E.; Ordonez-Moran, P.; Clevers, H.; Lutolf, M. P. Designer Matrices for Intestinal Stem Cell and Organoid Culture. *Nature* **2016**, *539*, 560–564.

(24) Weiss, P.; Garber, B. Shape and Movement of Mesenchyme Cells As Functions of the Physical Structure of the Medium-Contributions to a Quantitative Morphology. *Proc. Natl. Acad. Sci. U. S. A.* **1952**, *38*, 264–280.

(25) Crouzier, T.; Fourel, L.; Boudou, T.; Albiges-Rizo, C.; Picart, C. Presentation of BMP-2 from a Soft Biopolymeric Film Unveils Its Activity on Cell Adhesion and Migration. *Adv. Mater.* **2011**, *23*, H111–H118.

(26) DeForest, C. A.; Tirrell, D. A. A Photoreversible Protein-Patterning Approach for Guiding Stem Cell Fate in Three-Dimensional Gels. *Nat. Mater.* **2015**, *14*, 523–531.

(27) Stein, G. S.; Lian, J. B. Molecular Mechanisms Mediating Proliferation Differentiation Interrelationships during Progressive Development of the Osteoblast Phenotype. *Endocr. Rev.* **1993**, *14*, 424–442.

(28) Shi, X. T.; Li, L.; Ostrovidov, S.; Shu, Y. W.; Khademhosseini, A.; Wu, H. K. Stretchable and Micropatterned Membrane for Osteogenic Differentiation of Stem Cells. *ACS Appl. Mater. Interfaces* **2014**, *6*, 11915–11923.

(29) Khetan, S.; Guvendiren, M.; Legant, W. R.; Cohen, D. M.; Chen, C. S.; Burdick, J. A. Degradation-Mediated Cellular Traction Directs Stem Cell Fate in Covalently Crosslinked Three-Dimensional Hydrogels. *Nat. Mater.* **2013**, *12*, 458–465.

(30) Abdeen, A. A.; Lee, J.; Bharadwaj, N. A.; Ewoldt, R. H.; Kilian, K. A. Temporal Modulation of Stem Cell Activity Using Magnetoactive Hydrogels. *Adv. Healthcare Mater.* **2016**, *5*, 2536–2544.

(31) Liao, J. W.; Wu, S. L.; Yin, Z. Y.; Huang, S. S.; Ning, C. Y.; Tan, G. X.; Chu, P. K. Surface-Dependent Self-Assembly of Conducting Polypyrrole Nanotube Arrays in Template-Free Electrochemical Polymerization. *ACS Appl. Mater. Interfaces* **2014**, *6*, 10946–10951.

(32) Bai, H.; Shi, G. Q. Gas Sensors Based on Conducting Polymers. *Sensors* **2007**, *7*, 267–307.

(33) Cho, Y. N.; Borgens, R. Biotin-Doped Porous Polypyrrole Films for Electrically Controlled Nanoparticle Release. *Langmuir* **2011**, *27*, 6316–6322.

(34) Gao, M.; Dai, L. M.; Wallace, G. G. Biosensors Based on Aligned Carbon Nanotubes Coated with Inherently Conducting Polymers. *Electroanalysis* **2003**, *15*, 1089–1094.

(35) Zheng, W.; Razal, J. M.; Whitten, P. G.; Ovalle-Robles, R.; Wallace, G. G.; Baughman, R. H.; Spinks, G. M. Artificial Muscles Based on Polypyrrole/Carbon Nanotube Laminates. *Adv. Mater.* **2011**, *23*, 2966–2970.

- (36) Abidian, M. R.; Martin, D. C. Multifunctional Nanobiomaterials for Neural Interfaces. *Adv. Funct. Mater.* **2009**, *19*, 573–585.
- (37) Long, Y. Z.; Li, M. M.; Gu, C. Z.; Wan, M. X.; Duvail, J. L.; Liu, Z. W.; Fan, Z. Y. Recent Advances in Synthesis, Physical Properties and Applications of Conducting Polymer Nanotubes and Nanofibers. *Prog. Polym. Sci.* **2011**, *36*, 1415–1442.
- (38) Zhu, B.; Luo, S. C.; Zhao, H. C.; Lin, H. A.; Sekine, J.; Nakao, A.; Chen, C.; Yamashita, Y.; Yu, H. H. Large Enhancement in Neurite Outgrowth on a Cell Membrane-Mimicking Conducting Polymer. *Nat. Commun.* **2014**, *5*, 4523.
- (39) Park, J.; Bauer, S.; von der Mark, K.; Schmuki, P. Nanosize and Vitality: TiO₂ Nanotube Diameter Directs Cell Fate. *Nano Lett.* **2007**, *7*, 1686–1691.
- (40) Gandhi, M. R.; Murray, P.; Spinks, G. M.; Wallace, G. G. Mechanism of Electromechanical Actuation in Polypyrrole. *Synth. Met.* **1995**, *73*, 247–256.
- (41) Smela, E. Conjugated Polymer Actuators for Biomedical Applications. *Adv. Mater.* **2003**, *15*, 481–494.
- (42) Liu, M. J.; Liu, X. L.; Wang, J. X.; Wei, Z. X.; Jiang, L. Electromagnetic Synergetic Actuators Based on Polypyrrole/Fe₃O₄ Hybrid Nanotube Arrays. *Nano Res.* **2010**, *3*, 670–675.
- (43) Liu, W. T.; Wei, Y.; Zhang, X. H.; Xu, M. M.; Yang, X. P.; Deng, X. L. Lower Extent but Similar Rhythm of Osteogenic Behavior in hBMSCs Cultured on Nanofibrous Scaffolds *versus* Induced with Osteogenic Supplement. *ACS Nano* **2013**, *7*, 6928–6938.
- (44) Dalby, M. J.; Gadegaard, N.; Tare, R.; Andar, A.; Riehle, M. O.; Herzyk, P.; Wilkinson, C. D. W.; Oreffo, R. O. C. The Control of Human Mesenchymal Cell Differentiation Using Nanoscale Symmetry and Disorder. *Nat. Mater.* **2007**, *6*, 997–1003.
- (45) Douville, N. J.; Zamankhan, P.; Tung, Y. C.; Li, R.; Vaughan, B. L.; Tai, C. F.; White, J.; Christensen, P. J.; Grotberg, J. B.; Takayama, S. Combination of Fluid and Solid Mechanical Stresses Contribute to Cell Death and Detachment in a Microfluidic Alveolar Model. *Lab Chip* **2011**, *11*, 609–619.
- (46) Bershadsky, A. D.; Balaban, N. Q.; Geiger, B. Adhesion-Dependent Cell Mechanosensitivity. *Annu. Rev. Cell Dev. Biol.* **2003**, *19*, 677–695.
- (47) Liu, H. L.; Liu, X. L.; Meng, J. X.; Zhang, P. C.; Yang, G.; Su, B.; Sun, K.; Chen, L.; Han, D.; Wang, S. T.; et al. Hydrophobic Interaction-Mediated Capture and Release of Cancer Cells on Thermoresponsive Nanostructured Surfaces. *Adv. Mater.* **2013**, *25*, 922–927.
- (48) Bellanger, H.; Darmanin, T.; Taffin de Givenchy, E.; Guittard, F. Chemical and Physical Pathways for the Preparation of Superoleophobic Surfaces and Related Wetting Theories. *Chem. Rev.* **2014**, *114*, 2694–2716.
- (49) Hou, J. W.; Shi, Q.; Ye, W.; Stagnaro, P.; Yin, J. H. Micropatterning of Hydrophilic Polyacrylamide Brushes to Resist Cell Adhesion but Promote Protein Retention. *Chem. Commun.* **2014**, *50*, 14975–14978.
- (50) Lai, Y. K.; Gao, X. F.; Zhuang, H. F.; Huang, J. Y.; Lin, C. J.; Jiang, L. Designing Superhydrophobic Porous Nanostructures with Tunable Water Adhesion. *Adv. Mater.* **2009**, *21*, 3799–3803.
- (51) Engler, A. J.; Sen, S.; Sweeney, H. L.; Discher, D. E. Matrix Elasticity Directs Stem Cell Lineage Specification. *Cell* **2006**, *126*, 677–689.
- (52) Even-Ram, S.; Artym, V.; Yamada, K. M. Matrix Control of Stem Cell Fate. *Cell* **2006**, *126*, 645–647.
- (53) Ehrlicher, A. J.; Nakamura, F.; Hartwig, J. H.; Weitz, D. A.; Stossel, T. P. Mechanical Strain in Actin Networks Regulates FilGAP and integrin Binding to Filamin A. *Nature* **2011**, *478*, 260–263.
- (54) Wu, C. C.; Li, Y. S.; Haga, J. H.; Kaunas, R.; Chiu, J. J.; Su, F. C.; Usami, S.; Chien, S. Directional Shear Flow and Rho Activation Prevent the Endothelial Cell Apoptosis Induced By Micropatterned Anisotropic Feometry. *Proc. Natl. Acad. Sci. U. S. A.* **2007**, *104*, 1254–1259.
- (55) Wang, N.; Naruse, K.; Stamenovic, D.; Fredberg, J. J.; Mijailovich, S. M.; Tolic-Norrelykke, I. M.; Polte, T.; Mannix, R.; Ingber, D. E. Mechanical Behavior in Living Cells Consistent with the Tensegrity Model. *Proc. Natl. Acad. Sci. U. S. A.* **2001**, *98*, 7765–7770.
- (56) Kanchanawong, P.; Shtengel, G.; Pasapera, A. M.; Ramko, E. B.; Davidson, M. W.; Hess, H. F.; Waterman, C. M. Nanoscale Architecture of Integrin-Based Cell Adhesions. *Nature* **2010**, *468*, 580–584.
- (57) Dupont, S.; Morsut, L.; Aragona, M.; Enzo, E.; Giulitti, S.; Cordenonsi, M.; Zanconato, F.; Le Digabel, J.; Forcato, M.; Bicciato, S.; et al. Role of YAP/TAZ in Mechanotransduction. *Nature* **2011**, *474*, 179–183.
- (58) Azzolin, L.; Panciera, T.; Soligo, S.; Enzo, E.; Bicciato, S.; Dupont, S.; Bresolin, S.; Frasson, C.; Basso, G.; Guzzardo, V.; et al. YAP/TAZ Incorporation in the Beta-Catenin Destruction Complex Orchestrates the Wnt Response. *Cell* **2014**, *158*, 157–170.
- (59) Sun, Y. B.; Yong, K. M. A.; Villa-Diaz, L. G.; Zhang, X. L.; Chen, W. Q.; Philson, R.; Weng, S. N.; Xu, H. X.; Krebsbach, P. H.; Fu, J. P. Hippo/YAP-Mediated Rigidity-Dependent Motor Neuron Differentiation of Human Pluripotent Stem Cells. *Nat. Mater.* **2014**, *13*, 599–604.
- (60) Halder, G.; Dupont, S.; Piccolo, S. Transduction of Mechanical and Cytoskeletal Cues by YAP and TAZ. *Nat. Rev. Mol. Cell Biol.* **2012**, *13*, 591–600.
- (61) Zhu, Y.; Mao, Z. W.; Gao, C. Y. Control over the Gradient Differentiation of Rat BMSCs on a PCL Membrane with Surface-Immobilized Alendronate Gradient. *Biomacromolecules* **2013**, *14*, 342–349.
- (62) Kabeche, L.; Compton, D. A. Cyclin A Regulates Kinetochores Microtubules to Promote Faithful Chromosome Segregation. *Nature* **2013**, *502*, 110–113.